Progress In Electromagnetics Research C, Vol. 132, 187–203, 2023

Design of Miniaturized Tri-Band Wearable Antenna Based on Characteristic Mode Theory

Mingqing Wang[1], Zhonggen Wang[1], Ming Yang[2, *], Wenyan Nie[3], and Han Lin[1]

Abstract—In this study, a tri-band wearable antenna with a metal frame of $36 \times 36 \times 6.6\,\text{mm}^3$ is designed, fabricated, and measured based on the characteristic mode theory. By analyzing the current and electric field distribution of the characteristic mode, the antenna is determined to be fed by a T-coupled structure. Moreover, a circular ring ground structure is added to the initial elliptical model structure to generate a new resonance in the n78 band. On the other hand, the current's path is changed by etching a rectangular slot, allowing the high-frequency resonance mode to be shifted to the right. Simulated and measured results show that the proposed antenna covers Bluetooth/Wi-Fi (2.4G, 5.8G) and N78 frequency bands, which can be respectively used for connecting a watch to a mobile phone, accessing the Internet and making phone calls. Furthermore, the antenna has a maximum peak gain of 4.11 dBi in free space and 6.9 dBi when being placed on the wrist, with a Specific Absorption Rate (SAR) lower than international standards, making it suitable for wearable devices.

1. INTRODUCTION

In an intelligent era when people focus on health, smartwatches are made to be more lightweight and easy to carry [1–4], able to make calls and capable of performing other rich functions, such as sports records, getting rid of the relatively heavier cell phones carried during workout, which gradually increases people's interest in wearable devices [5–7]. In this context, High Impedance Surface (HIS) suppresses human body effect and builds low-profile antennas, suitable for the design of wearable antennas. However, HIS is significantly large in electrical characteristics, and although finite-size HIS antennas operating in 2.4G bands were proposed in [8–15], the integrated antenna structure is still large, and the overall size needs to be considered, which makes the antenna design difficult. In this setting, the characteristic mode theory was proposed half a century ago [16–18], giving theoretical support for antenna design, and it has been widely used in all kinds of antenna design [19–22]. In recent years, metal-bezel devices have received substantial attention from users and antenna design companies, and metal-bezel smartwatches have become increasingly popular [23–27]. Refs. [23, 24] both designed a 2×2 Multiple-Input Multiple-Output (MIMO) antenna based on the characteristic mode theory, although both antennas only worked under the 2.4 GHz band. Ref. [23] used a frame of circular metal to support an Fr4 substrate and changed the voltage zero point by modifying the shape of the circular ground edge so that the dual ports with orthogonal excitation present higher isolation, and the antenna has better free space and hand model. Furthermore, the antenna demonstrates superior radiation patterns, gain, and matching performance in both free space and hand models. However, the key parameter of SAR was not elaborated in the study. Ref. [24] designed a low SAR antenna with a higher efficiency than 86% and employed a square metal frame, successfully achieving a SAR of less than 1 W/kg by designing a feature where the current was

Received 26 February 2023, Accepted 23 April 2023, Scheduled 30 April 2023

* Corresponding author: Ming Yang (myang@ahu.edu.cn).

[1] School of Electrical and Information Engineering, Anhui University of Science and Technology, Huainan 232001, China. [2] School of Electrical and Communications Engineering, West Anhui University, Lu'an 237012, China. [3] School of Mechanical and Electrical Engineering, Huainan Normal University, Huainan 232001, China.

reversed between the frame and the ground and symmetric on both sides of the minimum [28]. Various designed antennas work on a single frequency band [29–34]. Some of them are costly to fabricate, and the process is extremely complicated. In the era of increasingly diverse communication methods, the vast majority of smartwatches realize the function of communication through the Operating System (OS), connecting to Wi-Fi or inserting a Subscriber Identity Module (SIM) card to access the Internet, also interconnecting with other smart terminals using Bluetooth. Hence, smartwatches need multiple antennas or multi-band antennas to support these functions [35–41].

In this study, a tri-band miniaturized antenna with a metal bezel based on an Fr4 substrate is proposed. For the initial structural model, the antenna is analyzed based on the characteristic mode theory. Thus, by analyzing the current distribution and electric field distribution of the resonant mode, it is clear that the T-coupling excitation is used to feed the antenna. Subsequently, add ground branches to add new resonance, and change the current path by etching the ground to affect the resonance mode. The results show that the suggested antenna with a symmetric structure covers Bluetooth, Wi-Fi (2.4G, 5.8G), and N78 bands. SAR indicators also complies with international standards.

The rest of the paper is organized as follows. Section 2 shows the proposed antenna's design evolution and presents the current distribution at the resonance point. Section 3 presents the parametric analysis in free space, and Section 4 presents the parametric analysis of the antenna on the hand model. Finally, Section 5 gives the conclusions.

2. DESIGN PROCESS OF THE ANTENNA ELEMENTS

As shown in Figure 1, the initial structure of the proposed antenna is composed of three parts, an antenna radiator, a substrate made of Fr4, and an all-metal frame made of brass at the substrate's periphery. The detailed parameters of the model I dimensions are shown in Table 1. The radiation body is arranged in the lower layer of the dielectric substrate, consisting of a large ellipse and a symmetrically distributed combination of two small ellipses to 90° rotation replicated three times. The large ellipse's 10.5 mm long axis ratio is 2.5, while the small ellipse's 10 mm long axis ratio is 4. The angle formed between the long axis of the large ellipse and that of the small ellipse is 37°. The outer metal frame has an outer diameter D_1 of 36 mm, an inner diameter of 34 mm, and a height H_1 of 6.6 mm. The adopted dielectric substrate is $\varepsilon_r = 4.4$, $\tan\delta = 0.02$; the radius of the substrate is 17 mm; and the thickness H_2 is 0.8 mm. The simulations were modeled using the Computer Simulation Technology (CST) software, and the initial model was subjected to characteristic mode analysis. The Model Significance (MS) and Characteristic Angle (CA) of the first six modes are shown in Figures 2 and 3, respectively. From Figure 2, it can be seen that modes 1 and 2 resonate at 2.664 GHz, and modes 5 and 6 resonate at 5.256 GHz, while the MS of mode 4 is below 0.1. In Figure 3, the characteristic angle is around 270°, so mode 4 is difficult to excite.

Table 1. Proposed model I antenna size (mm).

D_0	D_1	R_1	R_2	H_1	H_2	R_3	R_4	P_1 (degree)
34	36	10.5	4.2	6.6	0.8	10	2.5	37

According to the Theory of Characteristic Modes (TCM) [42], how strongly a mode $\vec{J}_n$ is excited is determined by modal weighting coefficient α_n, which can be expressed as

$$\alpha_n = \frac{V_n^i}{1 + j\lambda_n} \tag{1}$$

where λ_n is the eigenvalue, and V_n^i is the modal excitation coefficient, which is defined by

$$V_n^i = \left\langle \vec{J}_n, \vec{E}^i \right\rangle = \oiint_S \vec{J}_n \cdot \vec{E}^i ds \tag{2}$$

where $\vec{E}^i$ is the impressed source.

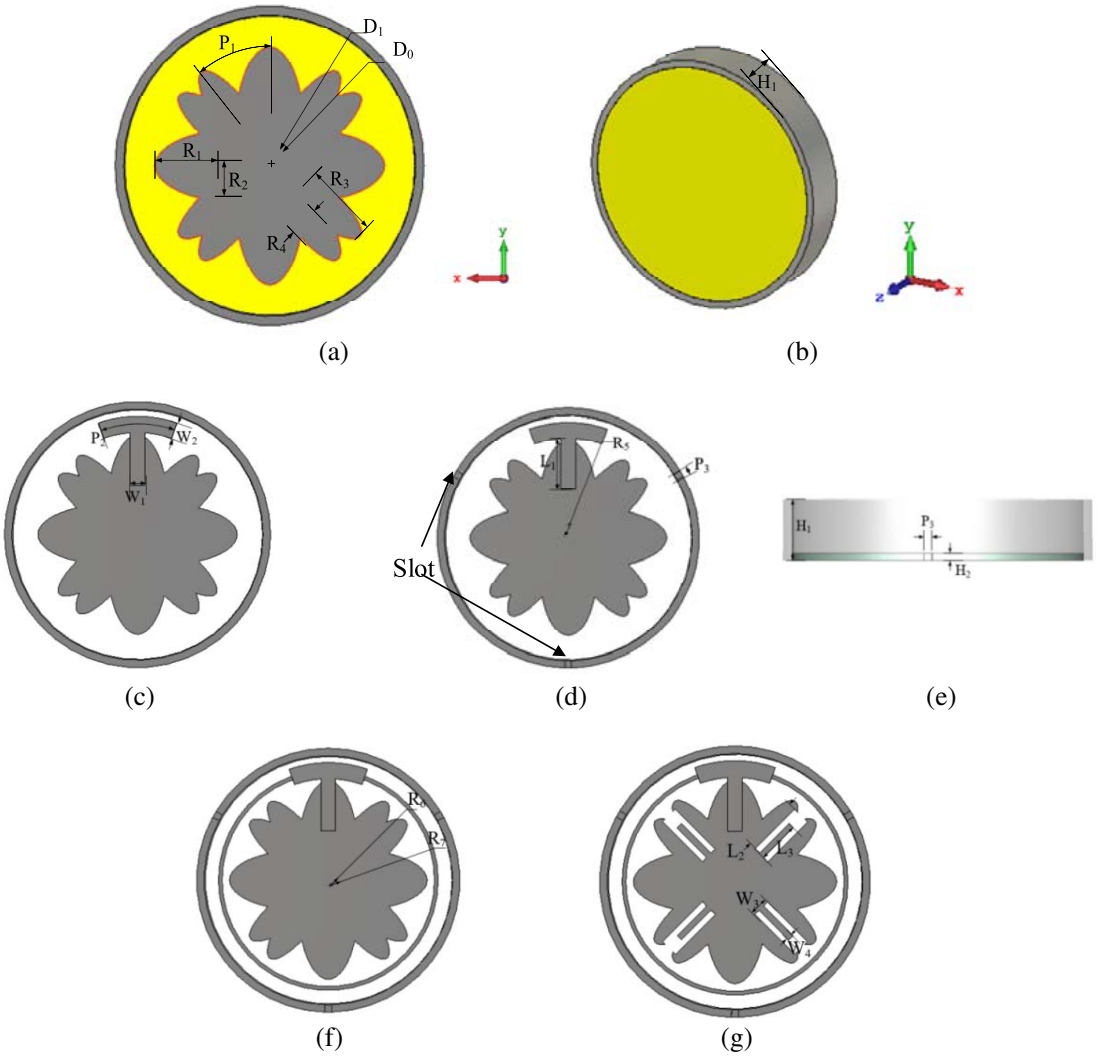

Figure 1. Antenna original model I: (a) Bottom view; (b) Side view; (c) Model II: Unslotted model; (d) Model II: Slotting model; (e) Side view model of slotting; (f) The proposed structural model III; (g) The proposed structural model IV.

For a specific mode, i.e., mode 1 in our case, its eigenvalue is fixed, so α_n totally depends on V_n^i. According to (2), to obtain a maximum coupling between the eigencurrent $\vec{J}_n$ and impressed source $\vec{E}^i$, the source should be placed at a current maximum, which is called inductive excitation [43].

Figure 4 shows the current distribution at the resonance modes of mode 1, mode 2, mode 5, and mode 6. The distributions of the currents prove that the current of mode 1 is in the vertical direction while the current of mode 2 is in the horizontal direction, and the distributions of the currents indicate that modes 1 and 2 are orthogonal.

TCM also tells us that if $\vec{E}^i$ is produced by an electric current $\vec{J}^i$, then reciprocal to (2) we have [42]

$$V_n^i = \left\langle \vec{E}_n, \vec{J}^i \right\rangle = \oiint_S \vec{E}_n \cdot \vec{J}^i ds \tag{3}$$

where $\vec{E}_n$ is the electric field caused by modal current $\vec{J}_n$. Therefore, to excite the CM $\vec{J}_n$, $\vec{J}^i$ should be placed at an electric field maximum or current minimum, which is called capacitive excitation [43]. By analyzing the characteristic mode of Model I, it is found that the maximum mode current is in the upper half of the large ellipse. In this setting, to obtain the ideal feed position, Figure 5 illustrates the

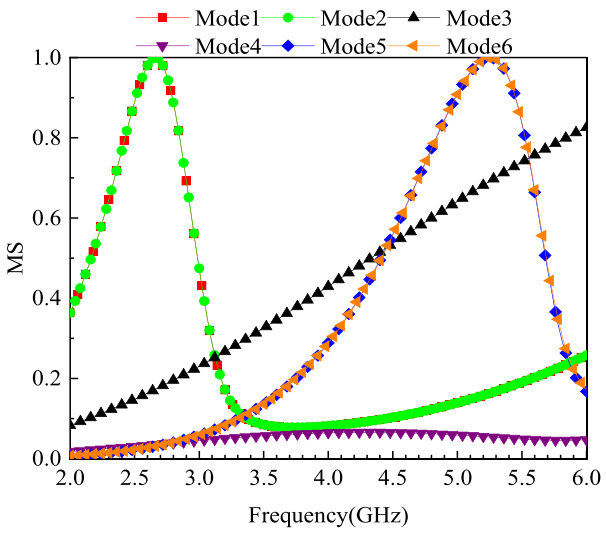

Figure 2. Model I for MS.

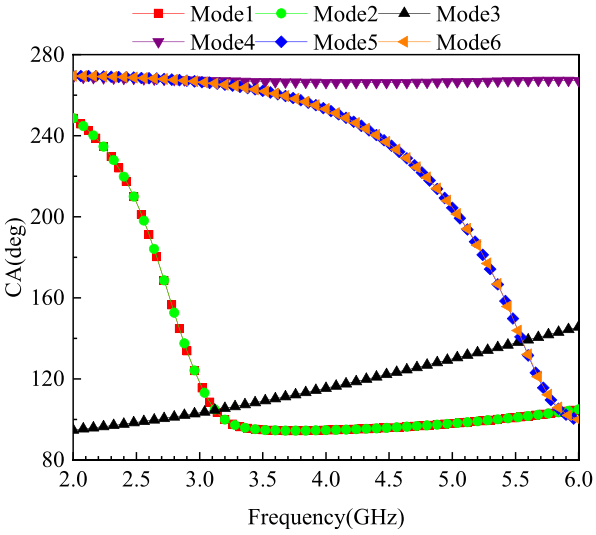

Figure 3. Model I for CA.

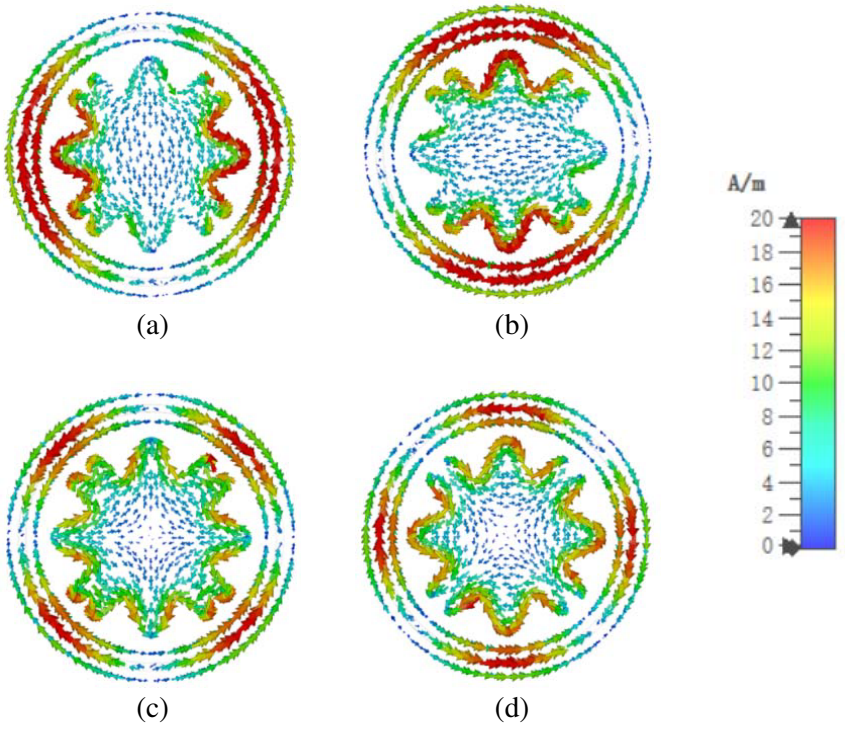

Figure 4. Current distribution of model I: (a) Mode 1; (b) Mode 2; (c) Mode 5; (d) Mode 6.

electric field distributions of the corresponding modes at the two resonance modes. It is obvious that for the resonant mode at low frequencies, there are two electric fields (voltage) maxima and two zero points along the gap between the metal frame and the ground; for resonance at high frequencies (mode 6), there are four electric fields (voltage) maxima and four zero points along the gap between the metal frame and the ground. Subsequently, for the low-frequency mode 1, capacitive feeds are not placed at B and D; for mode 2, feeds are not placed at A and C, while for high-frequency mode 5, the feed can be placed at positions A, B, C, or D; however, for mode 6, coupling feeds can only be placed on the 45° diagonal, i.e., at A_1, B_1, C_1, and D_1. Furthermore, Figures 5(c) and 5(f) show the zero electric field

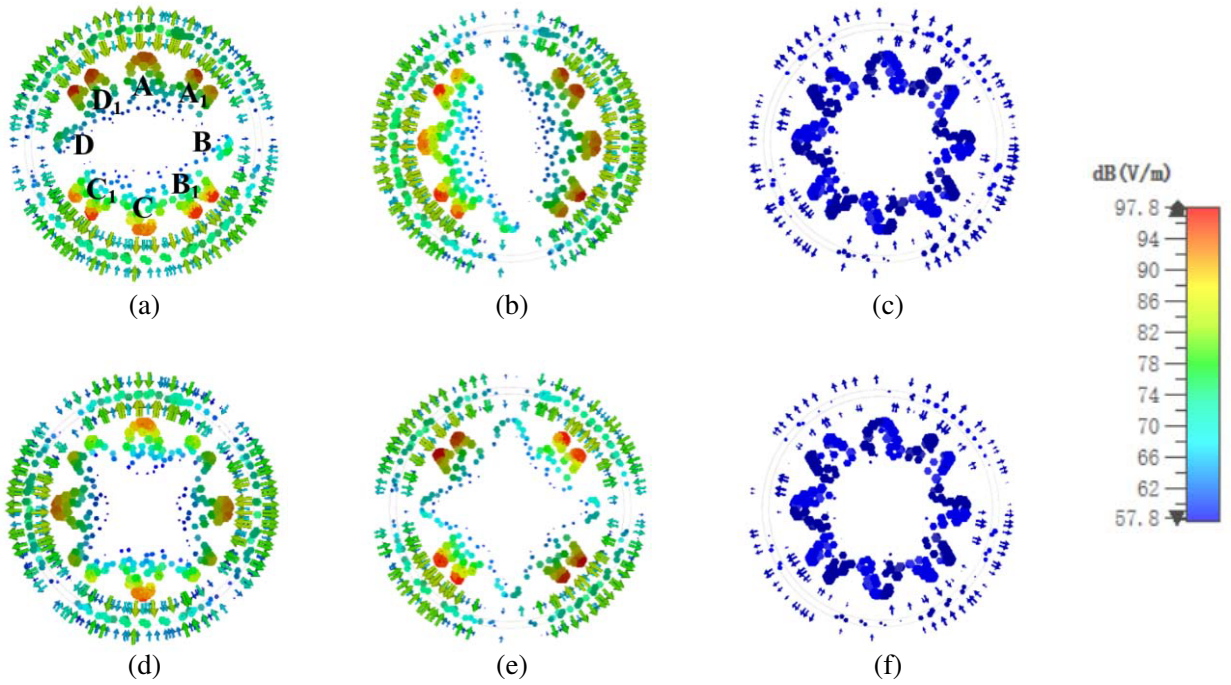

Figure 5. Electric field distribution of model I: (a) Mode 1 at 2.664 GHz; (b) Mode 2 at 2.664 GHz; (c) Mode 3 at 2.664 GHz; (d) Mode 5 at 5.256 GHz; (e) Mode 6 at 5.256 GHz; (f) Mode 3 at 5.256 GHz.

distribution of mode 3 at the resonance mode, which cannot be excited properly using the capacitive excitation method. Note that the MS value of mode 4 cannot be excited because it is relatively low. To excite the low and high frequencies, the coupling feed points at A and C need to be placed, and the capacitive excitation is more appropriate because the coupling feed is implemented easily between the ground and the metal frame.

As shown in Figure 1(c), for model II, a radiator was added to the substrate's upper surface, consisting of a rectangle and a circular arc: a T-shaped coupled feed structure and the port are expected to excite mode 1 and mode 5. The MS by the Characteristic Modes Analysis (CMA) model II, shown in Figure 6, reduces the resonance mode to 2.5 GHz for mode 1 and 4.66 GHz for mode 5. As illustrated in Figure 1(d), considering the actual deployment of the smartwatch, three small slits with a depth of 0.8 mm at 3° horizontally were cut from the metal frame to fix the substrate, and the slots were filled with Fr4 substrate to make a connection with the original circular substrate. The relevant parameters are represented in Table 2. Note that the feeder structure is above the large oval ground plane. The MS after slotting is shown in Figure 7. Moreover, comparing Figure 6 and Figure 7, the effect of the slit on the MS of the first 5 modes is neglected; however, the feed structure shifts the resonant frequencies to 2.496 GHz and 4.652 GHz. The currents at the resonance modes of the 4 modes are shown in Figure 8.

Table 2. Proposed model II antenna size after slotting (mm).

P_2	W_1	L_1	R_5	W_2	P_3	H_1	H_2
37°	2	7.3	13.8	2.2	3°	6.6	0.8

Various wearable devices nowadays support telephony, which requires the addition of corresponding calling bands, such as certain bands containing 5G. In this context, the multi-branch structure is used for a multi-frequency generation [44–46]. As shown in Figure 1(f), in this study, based on model II, a ring structure was added at the bottom of the substrate, called structure model III, whose relevant

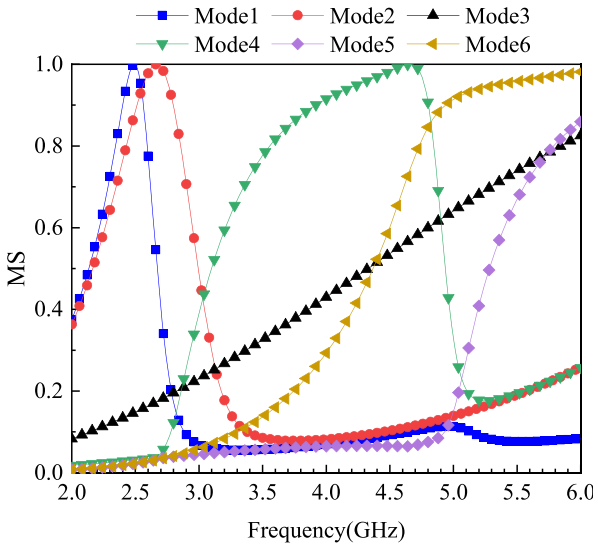

Figure 6. Distribution of MS of model II.

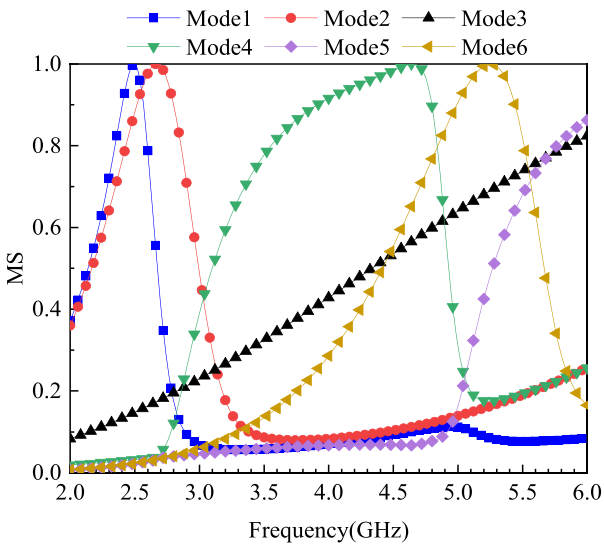

Figure 7. Distribution of MS of model II after slotting.

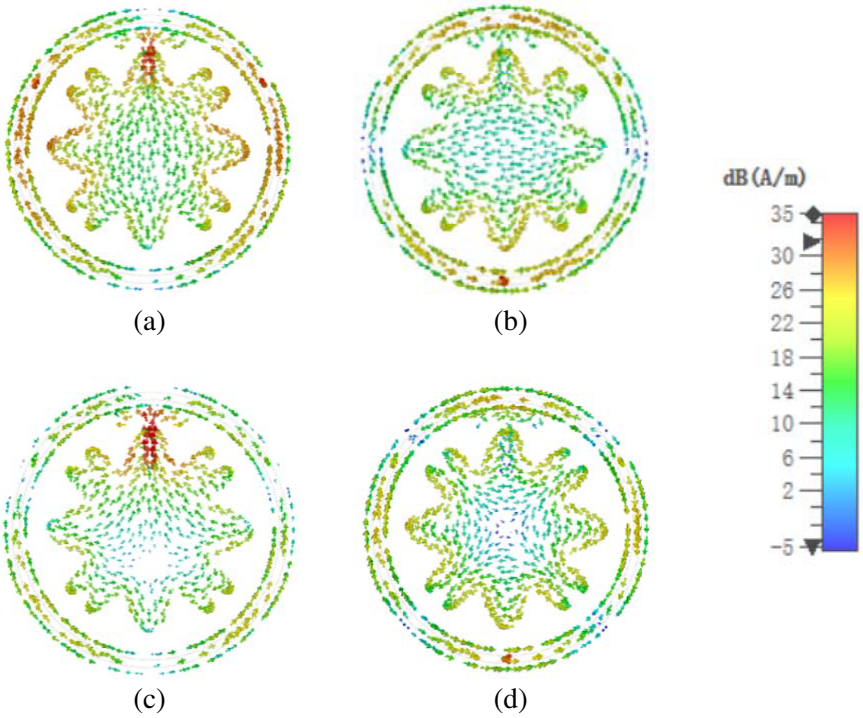

Figure 8. Current at resonance mode: (a) mode 1; (b) mode 2; (c) mode 4; (d) mode 6.

dimensions are presented in Table 3. A characteristic mode analysis for model III was performed, and the MS and CA data obtained by changing the dimensions of the circle are illustrated in Figure 9 and Figure 10. It is concluded that the resonance mode decreases slowly when the radius R_5 increases by 1 mm. The comparison shows that the circle radius is close to the requirement of the proposed design at 15 mm, and the width is equal to 1 mm. However, the resonance mode of the high frequency is low and does not resonate in the Wi-Fi 5G band. Subsequently, it is necessary to etch the slot or change other dimensions to improve the resonance of the high frequency.

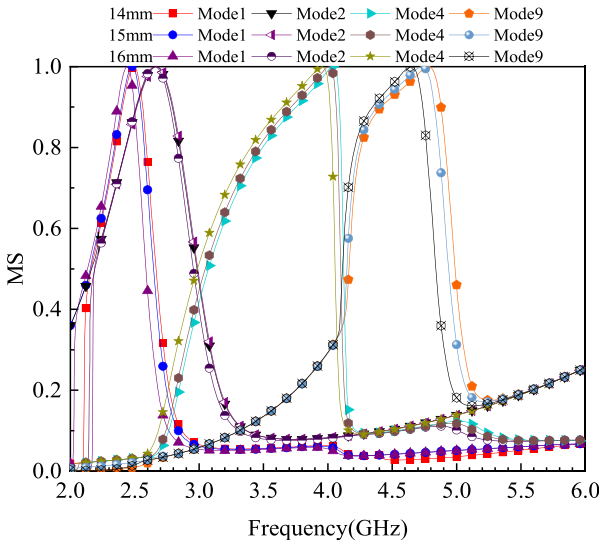

Figure 9. MS distribution of model III resonance modes at different R_7.

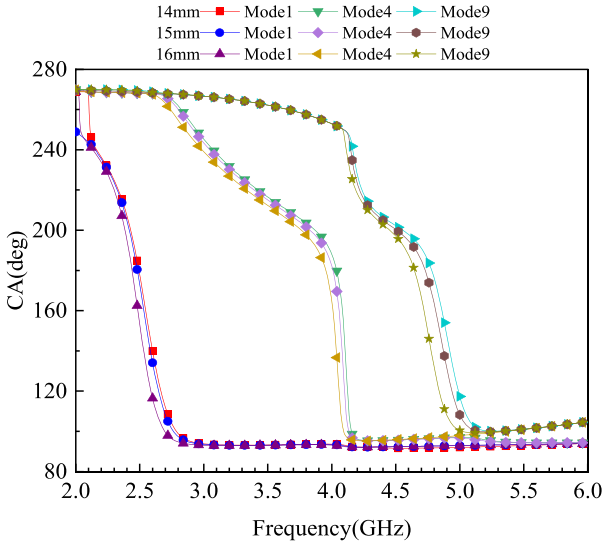

Figure 10. CA distribution of model III resonance modes at different R_7.

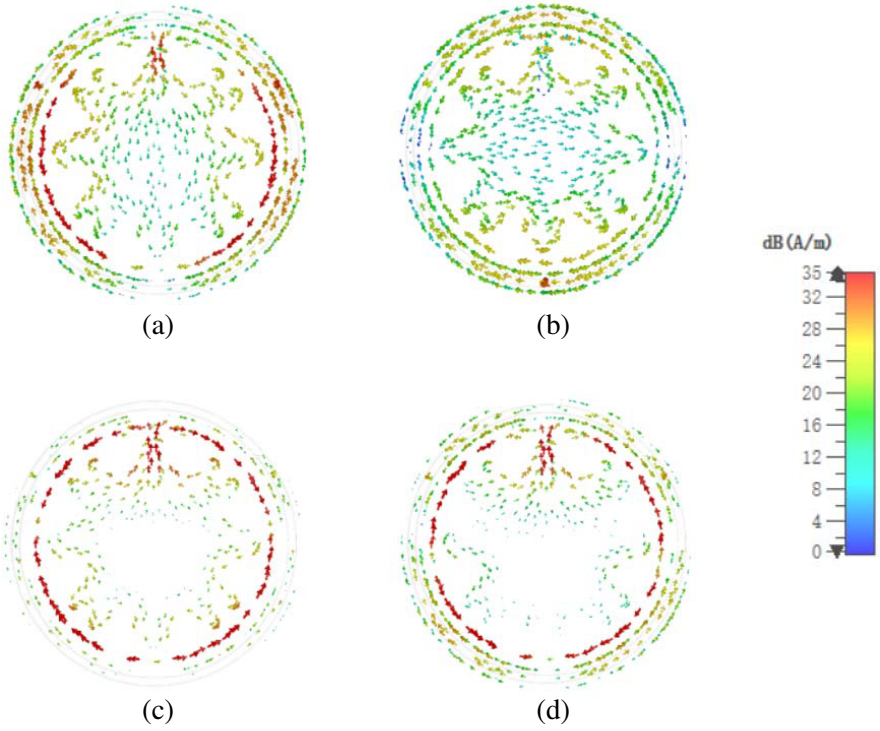

Figure 11. Resonance mode current distribution for model III: (a) Mode 1; (b) Mode 2; (c) Mode 4; (d) Mode 9.

Table 3. Proposed model III and model IV antenna sizes (mm).

R_6	R_7	L_2	L_3	W_3	W_4
14.5	15	7.6	6.5	2.4	0.8

Focusing on the characteristic patterns of model III, the four patterns with the MS are found close to 1. The resonance modes of mode 1 and mode 2 at low frequencies are respectively 2.48 GHz and 2.668 GHz, and the added ring makes the antenna add a resonance mode of 4 GHz at mid-frequencies, while the high-frequency resonance mode is lowered to nearly 4.7 GHz. Furthermore, Figure 11 illustrates the current distributions at the four modes' resonance modes. Hence, the currents of each mode are distributed on the increased circular ring, as well as the aforementioned T-shaped coupling structure. Consequently, it is concluded that mode 1, mode 4, and mode 5 are easily coupled to be excited while mode 2 is not easily excited.

To make the resonance mode of mode 5 at high frequencies shift to the right, slots were cut at diagonally opposite small ellipses touching each other, to change the current distribution state flowing through this place, thus changing the mode's distribution. Therefore, at the intersection of the two small ellipses, a U-shaped groove with an inward opening was etched to separate the intersection of the small ellipses. At this point, the model was called model IV, as shown in Figure 1(g). On the other hand, Table 3 provides the relevant dimensions of model IV. By analyzing structure IV, Figure 12 shows the MS distribution in the frequency band of interest; mode 1 resonates at 2.404 GHz, mode 4 at 3.528 GHz, and mode 11 at 5.764 GHz. Figure 13 illustrates the current distributions of the three resonance modes in the proposed frequency band.

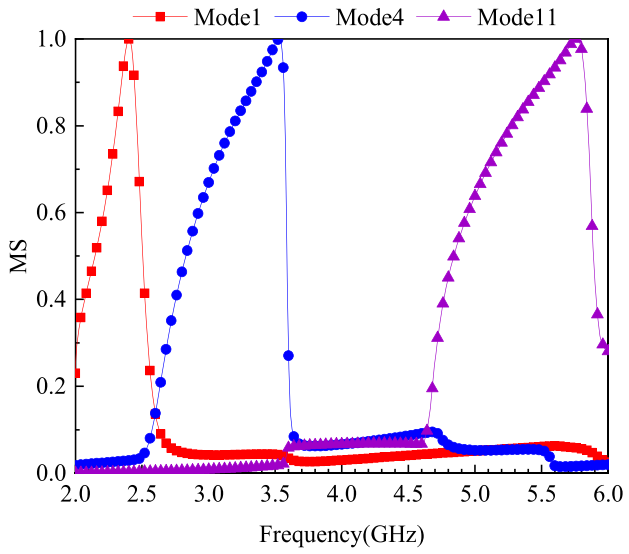

Figure 12. Distribution of interested MS.

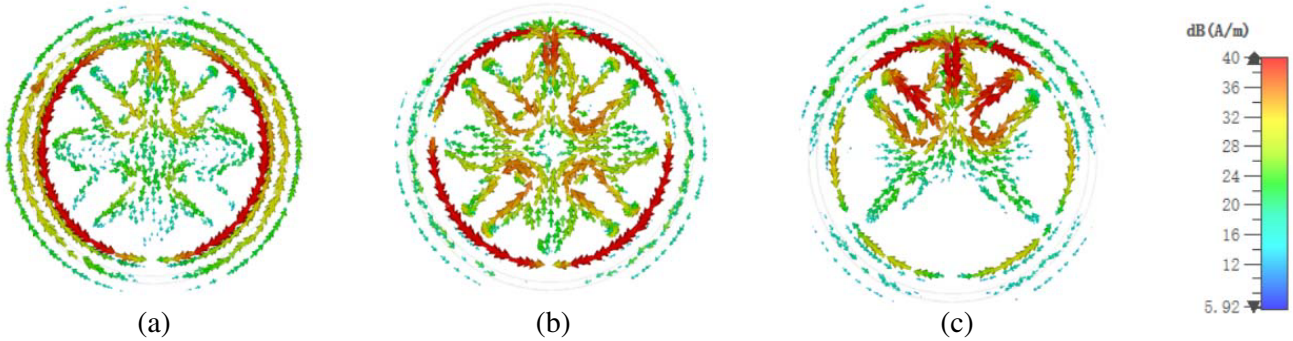

Figure 13. Current distribution at the MS resonance mode of interest: (a) Mode 1; (b) Mode 4; (c) Mode 11.

3. ANTENNA PERFORMANCE

3.1. Antenna Model Practical Measurement

The characteristic modes of model IV were calculated using the CST to observe the distribution of resonant mode currents, while the HFSS simulation software was employed for coupled feeds to excite mode 1, mode 4, and mode 11 with a 50 Ω coaxial feed. Figure 14 shows the model's physical diagram, while the measured environment is illustrated in Figure 15, with S-parameters measured via the AV3629D vector network analyzer. Figure 16(a) exhibits the S_{11} results after adding the excitation. The simulated and measured results show that the simulated and measured proposed antenna covers three bands of 2.4–2.48 GHz, 3.4–3.6 GHz, and 5.72–5.83 GHz under the standard of −10 dB. Note that the variability between the simulated and measured results may be due to the manufacturing process and welding errors. However, in general, they tend to be consistent.

Figure 14. Front and back view of the proposed antenna.

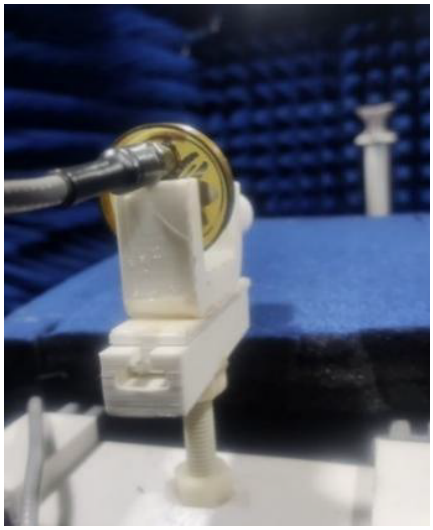

Figure 15. The environment of the antenna measurement.

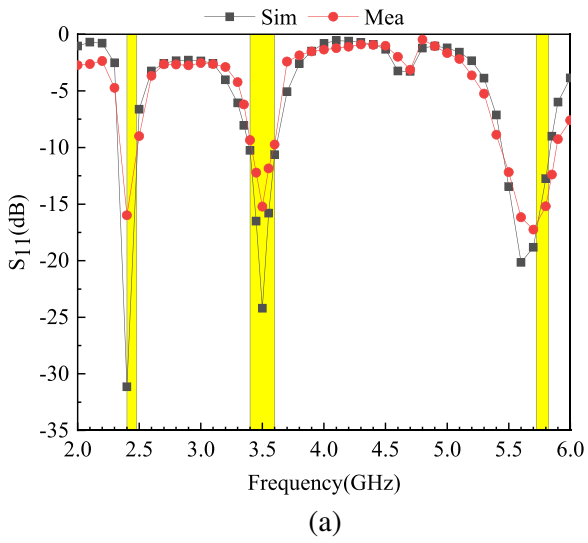

Figure 16. (a) Simulated and measured S-parameters; (b) Simulated and measured peak gains of the proposed antenna.

On the other hand, Figure 16(b) shows the antenna's gain in free space, which varies in the range of 1.8–4.11 dBi in the operating band. Model IV's gain tends to be stable in the operating band, although it may fluctuate unstably in multiple ranges. Figure 17 illustrates the actual measured and simulated EH direction diagrams at the resonance mode in an anechoic environment. In this setting, the E surface antenna directional map is basically a full radiation pattern; on the H surface, the pattern resembles the shape of an "8", and the two-way radiation effect is clear.

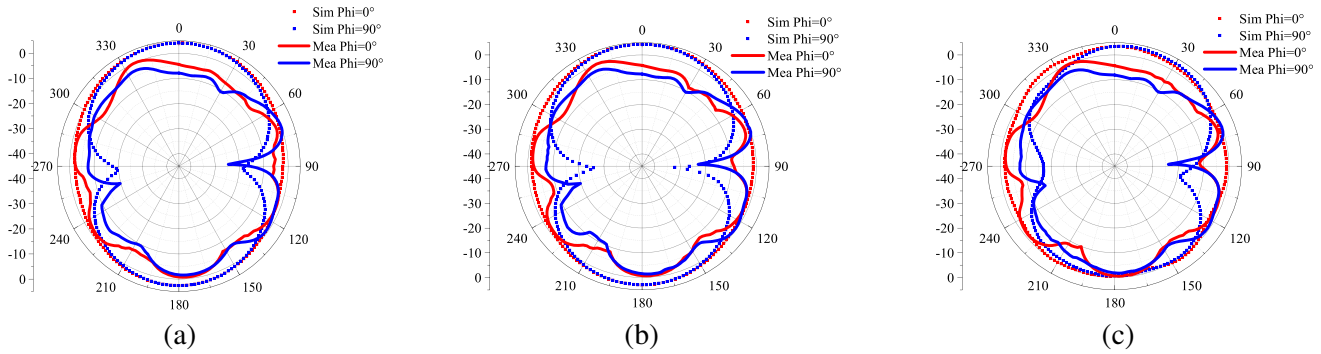

Figure 17. Simulated and measured far-field patterns on XOZ and YOZ planes at: (a) 2.4 GHz; (b) 3.5 GHz; (c) 5.8 GHz.

3.2. Parametric Study

A systematic study was carried out to investigate the effect of different parameters of the antenna on its performance. The purpose was to determine the manufacturing tolerances and, more importantly, to determine the effect of the parameters of the antenna on the bandwidth. Four parameters were studied, namely, the height H_2 of the metal frame, the long diameter R_1 of the large ellipse, the angle P of the rotation of the small ellipse, and the outer radius R_7 of the ring. The first two parameters were chosen because they lay the framework of the antenna's structure, while the last two correspond to the evolutionary redesign process of the antenna.

The height of the metal frame has a critical impact on the overall dimensions of the antenna, as evidenced by Figure 18, which illustrates the effect of different heights on the performance of S_{11}. It is

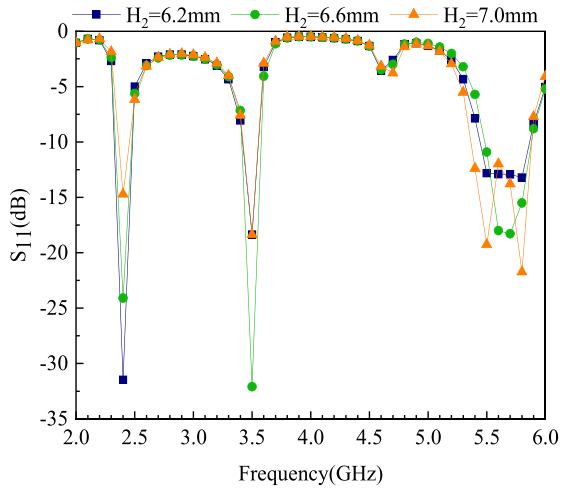

Figure 18. Effect of frame height H_2 on S-parameters.

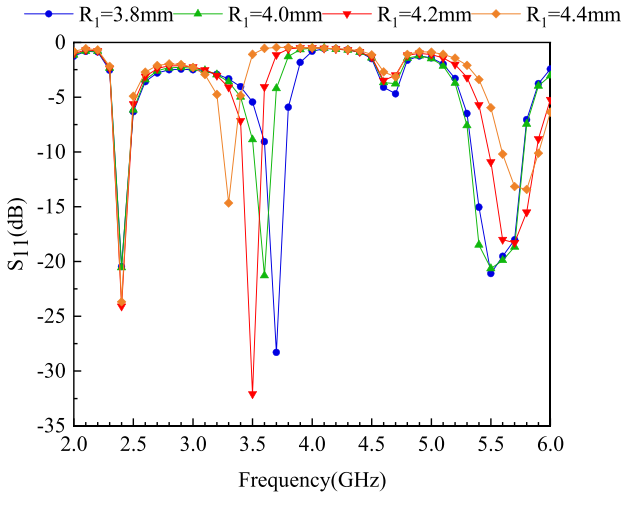

Figure 19. Effect of large elliptical diameter R_1 on S-parameters.

clear from the graph that when other parameters remain unchanged, the height changes from 6.2 mm to 7 mm: At low frequencies, the increase in height leads to a decrease in matching and coverage of the band, while at high frequencies the opposite occurs. Thus, the height of H_2 is equal to 6.6 mm. Figure 19 shows the effect of the long diameter R_1 of the large ellipse on the performance. It is seen in the figure that R_1 has a high influence on the antenna's resonance in the middle frequency and high frequency. With the change of radius R_1 from 3.8 mm to 4.4 mm, the resonance of the middle frequency decreases from 3.7 GHz to 3.3 GHz, the resonance mode of the high-frequency part moves from 5.5 GHz to 5.8 GHz, and the matching effect worsens. Through screening, it is found that R_1 is able to cover the target frequency band when taking 4.2 mm.

Figure 20 illustrates the effect of the rotation angle P_0 of the small ellipse on the performance of S_{11}. When the rotation angle P_0 increases, it mainly affects the high-frequency coverage, shifting the high-frequency resonance mode to the left. As for the low and medium frequency bands, the increased angle brings a finer matching effect. Subsequently, here, the angle is chosen as 37°, which achieves a satisfactory effect. Figure 21 exhibits the effect of the outer radius R_7 of the ring on the performance of S_{11}. By comparison, it is clear that the resonance mode decreases when R_7 increases, which corresponds to the descriptions of Figure 11 and Figure 12 earlier in this study. Increasing the size makes the resonance mode decrease. Hence, to ensure the coverage of the target frequency band, the size of R_7 is chosen as 15 mm.

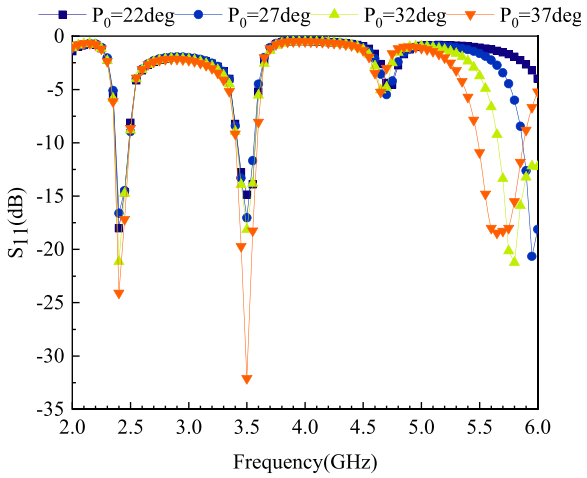

Figure 20. The effect of the angle P_0 of the small ellipse rotation on S-parameters.

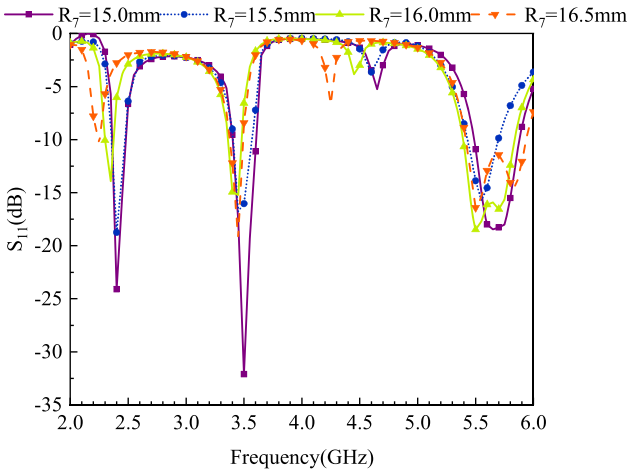

Figure 21. Effect of the circle radius R_7 on S-parameters.

4. SAR ASSESSMENT

As shown in Figure 22(a) below, the left-hand model was invoked in the HFSS software to simulate the antenna being worn on the hand. Moreover, the impedance bandwidth, gain, and directional maps were tested on both the free-space and human models. In this setting, consider the model with a watch on in the real case. The antenna was placed about 3 mm above the hand. To test the S-parameters of the antenna at the wrist, as in Figure 22(b), foam with a thickness of 3 mm was placed between the antenna and the hand, and the coaxial cable is bent and connected to the AV3629D vector network analyzer. The simulated and measured S_{11} are shown in Figure 23. Note that the antenna still covers the three bands mentioned in free space with the -6 dB criterion.

Electromagnetic waves have a certain radiation to human body. For antenna gain measurement of handheld devices, human safety issues are very critical and need to comply with the corresponding ICNIRP safety standards and other standards, so in the operating band of the antenna, we fix the hand model on the tester's wrist and place it in our Electromagnetic Compatibility (EMC) shielded acoustic chamber for testing, while in the non-operating band, its testing uses the hand model. In the next

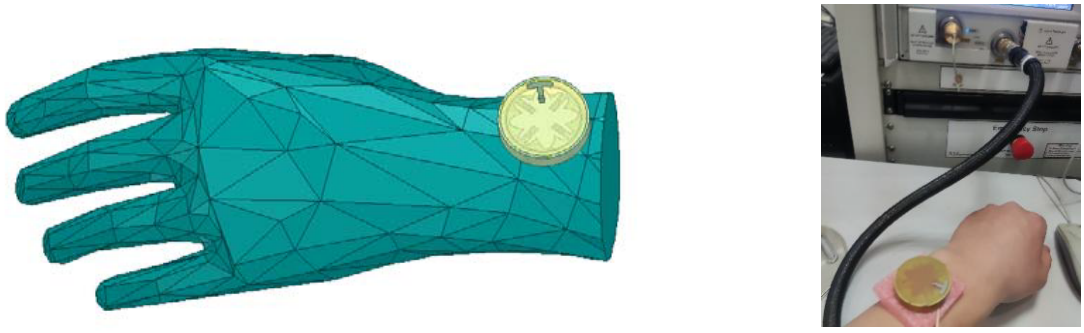

(a) (b)

Figure 22. Proposed smart watch antenna: (a) Simulation on human tissue model of HFSS; (b) Measured on human wrist.

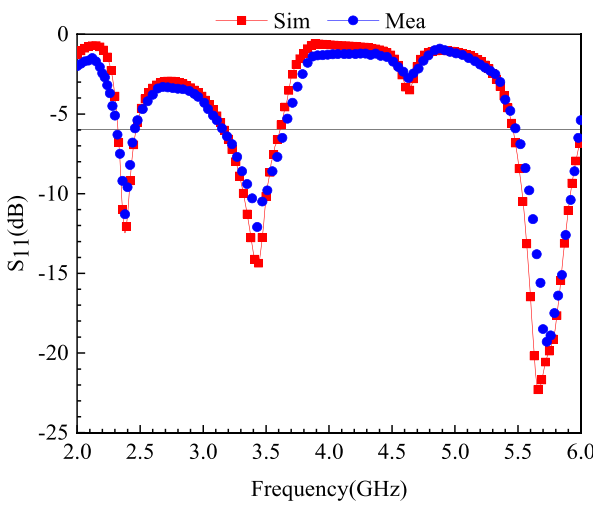

Figure 23. *S*-parameters simulated and measured on human tissue.

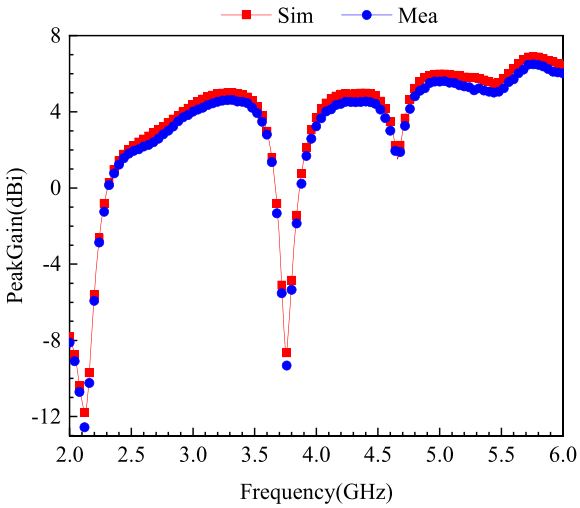

Figure 24. Peak gain simulated and measured on human tissue.

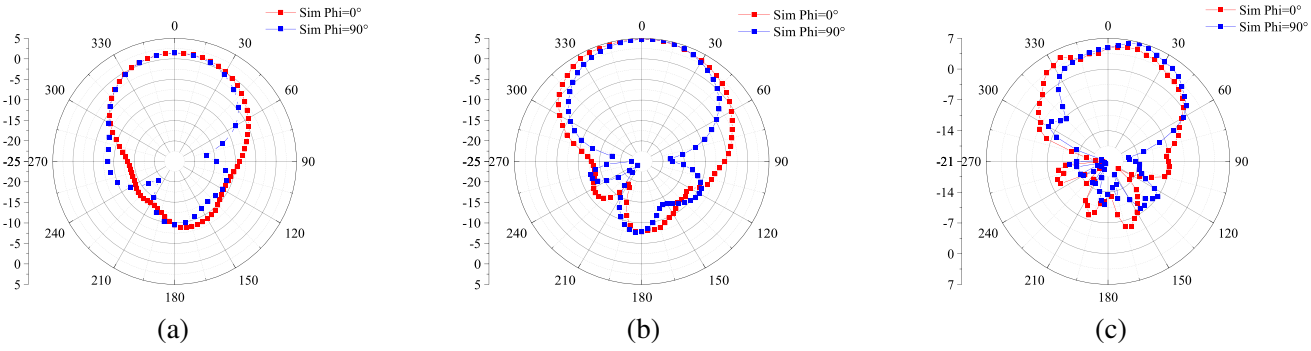

Figure 25. 3D pattern of the resonance mode during simulation on the hand model at: (a) 2.4 GHz; (b) 3.5 GHz; (c) 5.8 GHz.

section of this paper, we also study the effect of SAR on human body. As shown in Figure 24, the simulated low-frequency gain is 1.44–2.02 dBi; the mid-frequency gain is 2.97–4.89 dBi; and the gain in the high-frequency part is 6.79–6.9 dBi in the operating band range. Figure 25 illustrates the resonance mode in the simulation, as well as the direction of the measured EH surface map. The figure shows that

the three resonance modes are manifested in the directional radiation mode. Although the resonance mode on the H surface and the high-frequency resonance mode on the E surface have side lobes, they are smaller than the main lobe and will not affect the main radiation mode.

The designed antenna was placed 3 mm above the wrist, and the proposed antenna's 10 g peak body SAR at 2.4 GHz, 3.5 GHz, and 5.8 GHz was simulated; the total input power was set to 20 dBm. Figure 26 shows the 10 g peak average body SAR distribution, where the 10 g peak body SAR values of the antenna are all inferior to 2 W/kg when its port is excited.

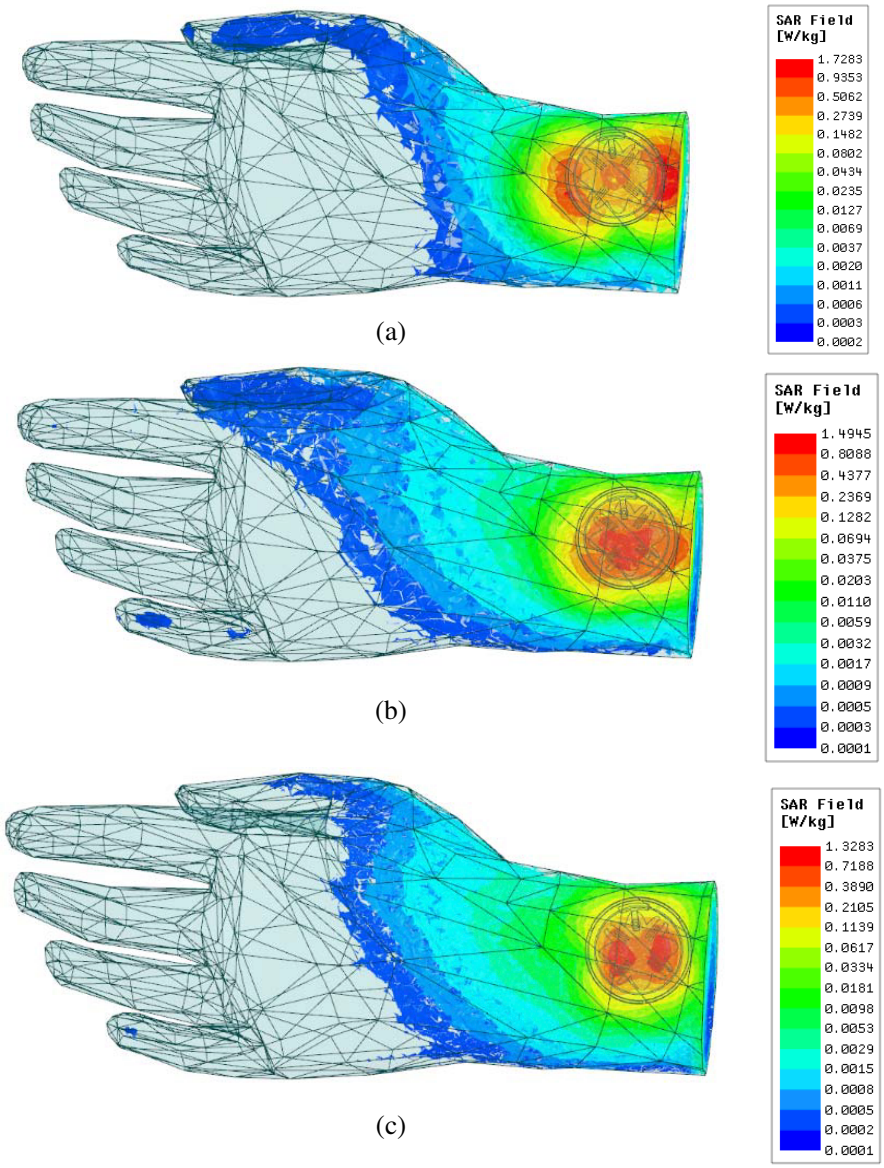

Figure 26. SAR value at resonance mode, at: (a) 2.4 GHz; (b) 3.5 GHz; (c) 5.8 GHz.

Table 4 compares this study with the existing literature in terms of size, bandwidth, gain, etc. The suggested antenna is of moderate size, and it covers three frequency bands. Subsequently, it is applied to Bluetooth, Wi-Fi (2.4 GHz and 5.8 GHz), and n78 bands. The antenna is placed on the hand model with a maximum peak gain of 6.9 dBi, and the SAR meets international standards.

Table 4. Antenna parameter comparison.

Ref.	Size (mm^3)	CMA	Metal Frame	Peak gain (dBi) Hand /No Hand	SAR (Min) (W/kg)	Application
[23]	7125.13	YES	YES	3.5/2	No	Bluetooth/WIFI(2.4G)
[24]	9072	YES	YES	No	0.73	Bluetooth/WIFI(2.4G)
[26]	8400	No	YES	No	No	GPS(L1), Bluetooth/WIFI(2.4G)
[27]	10000	No	YES	3.8/No	No	Bluetooth/WIFI(2.4G)
[31]	4069.44	No	No	2.801/3.476	0.2	WCDMA
[35]	16178.4	YES	No	4.5/No	No	GPS(L1), WIFI(2.4G), 5G(3.5 GHz, 4.9 GHz)
[36]	16820	YES	YES	No	0.86	GPS, Bluetooth/WIFI(2.4G), 5G(3.5 GHz, 4.9 GHz)
[40]	11025.568	YES	No	5.7/4.41	No	LTE, GSMBT, WIFI(2.4G)
This Work	6717.982	YES	YES	4.11/6.9	1.3283	WIFI(2.4G, 5.8G)/ Bluetooth, 5G(N78)

5. CONCLUSIONS

In this study, a miniaturized tri-band wearable antenna is designed based on the characteristic mode theory. The model consists of a radiator, an all-metal frame, and an Fr4 substrate, where the top of the metal frame has three equally spaced thin slots supporting the substrate. Moreover, simulations and measured tests show that the antenna covers Bluetooth, Wi-Fi (2.4 GHz and 5.8 GHz), and 5G bands (N78). When the antenna is placed in free space, it shows omnidirectional radiation on the E plane and bi-directional radiation on the H plane with a maximum gain of 4.11 dBi. On the contrary, when it is placed on the hand, it shows a directional radiation pattern, and the maximum gains in the three operating bands are 2.02 dBi, 4.89 dBi, and 6.89 dBi, respectively. SAR complies with international standards. Based on the above characteristics, it is capable of being used in smartwatches.

ACKNOWLEDGMENT

This work was supported in part by the Anhui Provincial Natural Science Foundation of China under Grant No. 2108085MF200, in part by the Natural Science Foundation of Anhui Provincial Education Department under Grant No. 2022AH051583 and No. KJ2020A0307, and the Graduate Innovation Fund of Anhui University of Science and Technology under Grant No. 2022CX2082.

REFERENCES

1. Skrivervik, K. and J. Trajkovikj, "Some considerations on wearable antennas," *Int. Conf. Appl. Electromagn. Commun. (ICECom) 2013*, 1–3, Dubrovnik, Croatia, 2013.
2. Lyons, K. and H. Profita, "The multiple dispositions of on-body and wearable devices," *IEEE Pervasive Computing*, Vol. 13, No. 4, 24–31, 2014.

3. Hamouda, H., P. Le Thuc, R. Staraj, and G. Kossiavas, "Dualband MICS/WIFI small antenna for portable applications in telemedicine," *2013 IEEE Antennas and Propagation Society International Symposium (APSURSI)*, 2081–2082, Orlando, FL, USA, 2013.
4. Salonen, P., L. Sydanheimo, M. Keskilammi, and M. Kivikoski, "A small planar inverted-F antenna for wearable applications," *Digest of Papers. Third International Symposium on Wearable Computers*, 95–100, San Francisco, CA, USA, 1999.
5. Marie, C., D. Estève, J.-Y. Fourniols, C. Escriba, and E. Campo, "Smart wearable systems: Current status and future challenges," *Artificial Intelligence in Medicine*, Vol. 56, No. 3, 137–156, 2012.
6. Rungtai, L. and J. G. Kreifeldt, "Ergonomics in wearable computer design," *International Journal of Industrial Ergonomics*, Vol. 27, No. 4, 259–269, 2001.
7. Gharode, D., A. Nella, and M. Rajagopal, "State-of-art design aspects of wearable, mobile, and flexible antennas for modern communication wireless systems," *Int. J. Commun. Syst.*, Vol. 34, No. 15, 1–48, 2021.
8. Cure, D., T. M. Weller, and F. A. Miranda, "Study of a low-profile 2.4-GHz planar dipole antenna using a high-impedance surface with 1-D varactor tuning," *IEEE Transactions on Antennas and Propagation*, Vol. 61, No. 2, 506–515, 2013.
9. Pandey, Q., K. K. Katare, A. Biswas, and M. J. Akhtar, "Frequency switchable AMC loaded folded slot antenna for dual band operation," *2017 IEEE Applied Electromagnetics Conference (AEMC)*, 1–2, Aurangabad, India, 2017.
10. Zhu, S. and R. Langley, "Dual-band wearable textile antenna on an EBG substrate," *IEEE Transactions on Antennas and Propagation*, Vol. 57, No. 4, 926–935, 2009.
11. Ta, S. X. and I. Park, "Dual-band low-profile crossed asymmetric dipole antenna on dual-band AMC surface," *IEEE Antennas and Wireless Propagation Letters*, Vol. 13, 587–590, 2014.
12. Joubert, J., J. C. Vardaxoglou, W. G. Whittow, and J. W. Odendaal, "CPW-fed cavity-backed slot radiator loaded with an AMC reflector," *IEEE Transactions on Antennas and Propagation*, Vol. 60, No. 2, 735–742, 2012.
13. Raad, H. R., A. I. Abbosh, H. M. Al-Rizzo, and D. G. Rucker, "Flexible and compact AMC based antenna for telemedicine applications," *IEEE Transactions on Antennas and Propagation*, Vol. 61, No. 2, 524–531, 2013.
14. Palukuru, V. K., A. Pekonen, V. Pynttäri, R. Mäkinen, J. Hagberg, and H. Jantunen, "An inkjet-printed inverted-F antenna for 2.4-GHz wrist applications," *Microw. Opt. Technol. Lett.*, Vol. 51, No. 12, 2936–2938, 2009.
15. Chen, Y.-S. and T.-Y. Ku, "A low-profile wearable antenna using a miniature high impedance surface for smartwatch applications," *IEEE Antennas and Wireless Propagation Letters*, Vol. 15, 1144–1147, 2016.
16. Garbacz, R. and R. Turpin, "A generalized expansion for radiated and scattered fields," *IEEE Transactions on Antennas and Propagation*, Vol. 19, No. 3, 348–358, May 1971.
17. Harrington, R. and J. Mautz, "Theory of characteristic modes for conducting bodies," *IEEE Transactions on Antennas and Propagation*, Vol. 19, No. 5, 622–628, September 1971.
18. Harrington, R. and J. Mautz, "Computation of characteristic modes for conducting bodies," *IEEE Transactions on Antennas and Propagation*, Vol. 19, No. 5, 629–639, September 1971.
19. Cabedo, F. M., A. Valero-Nogueira, E. Antonino-Daviu, and M. Ferrando-Bataller, "Modal analysis of a radiating slotted PCB for mobile handsets," *2006 First European Conference on Antennas and Propagation*, 1–6, Nice, France, 2006.
20. Antonino, D., E. Suarez-Fajardo, C. A., M. Cabedo-Fabrés, and M. Ferrando-Bataller, "Wideband antenna for mobile terminals based on the handset PCB resonance," *Microw. Opt. Technol. Lett.*, Vol. 48, No. 7, 1408–1411, 2006.
21. Deng, C., Z. Feng, and S. V. Hum, "MIMO mobile handset antenna merging characteristic modes for increased bandwidth," *IEEE Transactions on Antennas and Propagation*, Vol. 64, No. 7, 2660–2667, July 2016.

22. Manteuffel, D. and R. Martens, "Compact multimode multielement antenna for indoor UWB massive MIMO," *IEEE Transactions on Antennas and Propagation*, Vol. 64, No. 7, 2689–2697, July 2016.
23. Wen, D., Y. Hao, H. Wang, and H. Zhou, "Design of a MIMO antenna with high isolation for smartwatch applications using the theory of characteristic modes," *IEEE Transactions on Antennas and Propagation*, Vol. 67, No. 3, 1437–1447, 2019.
24. Liu, X. Z., G. Yu, J. Chao, H. H. Zhang, and Y. Liu, "TCM-based low-SAR MIMO antenna for smartwatch applications," *2021 International Conference on Microwave and Millimeter Wave Technology (ICMMT)*, 1–3, Nanjing, China, 2021.
25. Zhang, X., et al., "Analysis and design of stable-performance circularly-polarized antennas based on coupled radiators for smart watches," *IEEE Transactions on Antennas and Propagation*, Vol. 70, No. 7, 5312–5323, 2022.
26. Yan, Y., J. Ouyang, A. Sharif, Q. Wang, and Y. Ban, "Dual-loop antenna with band-stop circuit for GPS/Bluetooth metal-rimmed smartwatch applications," *2018 IEEE International Symposium on Antennas and Propagation & USNC/URSI National Radio Science Meeting*, 455–456, Boston, MA, USA, 2018.
27. Su, S.-W. and Y.-T. Hsieh, "Integrated metal-frame antenna for smartwatch wearable device," *IEEE Transactions on Antennas and Propagation*, Vol. 63, No. 7, 3301–3305, July 2015.
28. Zhang, H. H., G. G. Yu, Y. Liu, Y. X. Fang, G. Shi, and S. Wang, "Design of low-SAR mobile phone antenna: Theory and applications," *IEEE Transactions on Antennas and Propagation*, Vol. 69, No. 2, 698–707, 2021.
29. Gao, X., Z. Zhang, W. Chen, Z. Feng, M. F. Iskander, and A.-P. Zhao, "A novel wrist wear dual-band diversity antenna," *2009 IEEE Antennas and Propagation Society International Symposium*, 1–4, North Charleston, SC, USA, 2009.
30. Trinh, L. H., T. Q. K. Nguyen, H. L. Tran, P. C. Nguyen, N. V. Truong, and F. Ferrero, "Low-profile horizontal omni-directional antenna for LoRa wearable devices," *2017 International Conference on Advanced Technologies for Communications (ATC)*, 136–139, Quy Nhon, Vietnam, 2017.
31. Kwak, S. I., D.-U. Sim, J. H. Kwon, and Y. J. Yoon, "Design of PIFA with metamaterials for body-SAR reduction in wearable applications," *IEEE Transactions on Electromagnetic Compatibility*, Vol. 59, No. 1, 297–300, 2017.
32. Flores-Cuadras, J. R., J. L. Medina-Monroy, R. A. Chavez-Perez, and H. Lobato-Morales, "Novel ultra-wideband flexible antenna for wearable wrist worn devices with 4G LTE communications," *Microw. Opt. Technol. Lett.*, Vol. 59, No. 4, 777–783, 2017.
33. Su, S.-W. and Y.-T. Hsieh, "Integrated LDS antenna for B13 and B4/B3/B2/B1 LTE operation in smartwatch," *Microw. Opt. Technol. Lett.*, Vol. 59, No. 4, 869–873, 2017.
34. Hong, C.-Y. and S.-H. Yeh, "Cellular antenna design with metallic housing for wearable device," *2016 IEEE 5th Asia-Pacific Conference on Antennas and Propagation (APCAP)*, 419–420, Kaohsiung, Taiwan, 2016.
35. Xiao, B., H. Wong, D. Wu, and K. L. Yeung, "Design of small multiband full-screen smartwatch antenna for IoT applications," *IEEE Internet of Things Journal*, Vol. 8, No. 24, 17724–17733, 2021.
36. Zhang, H. H., et al., "Design of low-sar and high on-body efficiency tri-band smartwatch antenna utilizing the theory of characteristic modes of composite PEC-lossy dielectric structures," *IEEE Transactions on Antennas and Propagation*, Vol. 71, No. 2, 1913–1918, 2023.
37. Chen, W.-S., G.-Q. Lin, G.-R. Zhang, and C.-Y.-D. Sim, "Multiband antennas for GSM/GPS/LTE/WLAN smart watch applications," *2017 Sixth Asia-Pacific Conference on Antennas and Propagation (APCAP)*, 1–3, Xi'an, China, 2017.
38. Ahmad, S., A. Ghaffar, X. J. Li, and N. Cherif, "A millimetre-wave tri-band antenna embedded on smart watch for wearable applications," *2021 International Symposium on Antennas and Propagation (ISAP)*, 1–2, Taipei, Taiwan, 2021.
39. Jin, Y. and J. Choi, "Bandwidth enhanced compact dual-band smart watch antenna for WLAN 2.4/5.2 GHz application," *2017 International Applied Computational Electromagnetics Society Symposium (ACES)*, 1–2, Suzhou, China, 2017.

40. Chen, C.-H., Y.-F. Lin, P.-W. Huang, H.-M. Chen, and C.-T. Liao, "Design of multi-band antenna for LTE wearable device with shared slots and radiators for smart watch," *Int. J. RF Microw. Comput. Aided Eng.*, Vol. 30, No. 11, 1–14, 2020.
41. Ahmad, S., H. Boubakar, S. Naseer, M. Ehsanul Alim, Y. Ali Sheikh, A. Ghaffar, A. J. A. Al-Gburi, and N. O. Parchin, "Design of a tri-band wearable antenna for millimeter-wave 5G applications," *Sensors*, Vol. 22, No. 20, 1–14, 2022.
42. Foudazi, A., H. R. Hassani, and S. M. A. Nezhad, "Small UWB planar monopole antenna with added GPS/GSM/WLAN bands," *IEEE Transactions on Antennas and Propagation*, Vol. 60, No. 6, 2987–2992, 2012.
43. Harrington, R. and J. Mautz, "Theory of characteristic modes for conducting bodies," *IEEE Transactions on Antennas and Propagation*, Vol. 19, No. 5, 622–628, Sep. 1971.
44. Martens, R., E. Safin, and D. Manteuffel, "Inductive and capacitive excitation of the characteristic modes of small terminals," *Proc. Loughborough Antennas Propag. Conf.*, 1–4, Nov. 2011.
45. Li, W. T., X. W. Shi, and Y. Q. Hei, "Novel planar UWB monopole antenna with triple band-notched characteristics," *IEEE Antennas and Wireless Propagation Letters*, Vol. 8, 1094–1098, 2009.
46. Painam, S. K. and C. M. Bhuma, "A compact hexa-band and UWB antenna using heptagon and nonagon rings with vertex feed," *2018 IEEE Indian Conference on Antennas and Propagation (InCAP)*, 1–4, Hyderabad, India, 2018.